frontiers | Frontiers in Materials

TYPE Original Research
PUBLISHED 20 March 2023
DOI 10.3389/fmats.2023.1126806

Check for updates

OPEN ACCESS

EDITED BY
Zhiqiang Dong,
Southeast University, China

REVIEWED BY
Jun-Jie Zeng,
Guangdong University of Technology, China
Daxu Zhang,
Shanghai Jiao Tong University, China

*CORRESPONDENCE
Taha A. El-Sayed,
taha.ibrahim@feng.bu.edu.eg
A. Deifalla,
ahmed.deifalla@fue.edu.eg

SPECIALTY SECTION
This article was submitted to Structural Materials, a section of the journal Frontiers in Materials

RECEIVED 18 December 2022
ACCEPTED 28 February 2023
PUBLISHED 20 March 2023

CITATION
El-said A, Awad A, El-Sayed TA, Özkılıç YO, Deifalla A and Tawfik M (2023), Crack sliding model for non-shear FRP-reinforced slender concrete elements under shear.
Front. Mater. 10:1126806.
doi: 10.3389/fmats.2023.1126806

COPYRIGHT
© 2023 El-said, Awad, El-Sayed, Özkılıç, Deifalla and Tawfik. This is an open-access article distributed under the terms of the Creative Commons Attribution License (CC BY). The use, distribution or reproduction in other forums is permitted, provided the original author(s) and the copyright owner(s) are credited and that the original publication in this journal is cited, in accordance with accepted academic practice. No use, distribution or reproduction is permitted which does not comply with these terms.

Crack sliding model for non-shear FRP-reinforced slender concrete elements under shear

Amr El-said[1], Ahmed Awad[2], Taha A. El-Sayed[3]*, Yasin Onuralp Özkılıç[4], A. Deifalla[5]* and Maged Tawfik[1]

[1]Department of Civil Engineering, The Higher Institute of Engineering, El Shrouk, Cairo, Egypt, [2]Faculty of Engineering, October University for Modern Sciences and Arts, Giza, Egypt, [3]Department of Structural Engineering, Shoubra Faculty of Engineering -Benha University, Cairo, Egypt, [4]Necmettin Erbakan University, Faculty of Engineering, Department of Civil Engineering, Konya, Turkey, [5]Structural Engineering and Construction Management Department, Future University in Engineering, Cairo, Egypt

Fiber-reinforced polymer (FRP)-reinforced concrete (RC) elements fail under one-way shear in a devastating and complicated manner with no adequate warning. In recent decades, there has been pioneering research in this area; however, there is no agreement among researchers regarding mechanically-based models. Thus, in this current study, a plasticity-based model is developed for FRP-RC elements under shear. A selected model was firstly assessed for its accuracy, consistency, and safety against an extensive experimental database. Secondly, a plasticity-based model (i.e., crack shear sliding model) was adapted, refined, and proposed for FRP-RC elements under one-way shear. The two proposed models were found to be reliable and more accurate with respect to selected existing methods. Modeling of FRP's axial rigidity is more consistent only under Young's modulus with respect to the experimental database. Several concluding remarks on the selected existing models are outlined and discussed to assist the future development of these models and design codes.

KEYWORDS

one-way shear, FRP, crack sliding model, plasticity, slender

1 Introduction

The dilemma of shear of reinforced concrete (RC) elements is an old problem. This dilemma lacks robust mechanical models based on physics and is affected by several mechanisms and parameters (Ali et al., 2021; Ebid and Deifalla, 2021; Alkhatib and Deifalla, 2022; Deifalla and Salem, 2022; Salem and Deifalla, 2022). Fiber-reinforced polymer (FRP)-RC elements increase the ambiguity further by adding several effects, including and not limited to FRP's linear behavior up to failure and the variability of FRP's Young's modulus (Hassan and Deifalla, 2015; Elmeligy et al., 2017; Deifalla, 2020c; Deifalla, 2021a; Deifalla, 2022). Thus, the complexity associated with developing a physically-based mechanical model is considerable and requires further investigation of new representation approaches (Deifalla and Ghobarah, 2010a; Deifalla et al., 2013; Deifalla et al., 2014; Deifalla, 2015; Deifalla et al., 2015). This is imperative to attaining a much deeper understanding of failure under shear and, consequently, a base for optimum shear provisions in terms of reduced materials, prolonged life span, and improved reliability (Deifalla and Ghobarah, 2010b; Deifalla and Ghobarah, 2014; Deifalla, 2020b; Deifalla, 2021b; Deifalla, 2021d).

Since the 1950s, developing a mechanical model with a physical basis for the shear strength of steel-RC elements has been an ongoing area of investigation, with several models developed. The first were empirically based on simplified ones (Zsutty, 1968), which included the basic variables of concrete compressive strength, flexure reinforcement ratio, and element depth and width. Those variables were considered significant for shear strength by many researchers (Leonhardt et al., 1964). Later, the size effect was investigated and considered in those models (Hedman et al., 1978; Bazant and Kim, 1984; Ghannoum, 1998). Thereafter, researchers have considered the following variables: effect of the maximum nominal aggregate size (Bentz, 2005), fracture energy (Bazant and Planas, 1998), and element shear slenderness (Zsutty, 1968). These empirical models have included effective variables based on the results of experimental investigation; however, little attention has been directed to modeling the actual shear mechanism and behavior. Recently, research has aimed at achieving a more profound comprehension of shear behavior (Vecchio and Collins, 1986; Muttoni and Fernández Ruiz, 2008; Tung and Tue, 2016). With technological advances in experimental measurements and numerical analysis, a more refined grasp can be gained of the contribution of each shear mechanism. Therefore, several mechanical models have been developed (Huber et al., 2016; Cavagnis, 2017; Cladera et al., 2017). There are a handful of these in the literature for steel-RC elements under one-way shear, including but not limited to a compression chord model (Zink, 1999; Zararis and Papadakis, 2001). A compression field assumes that the governing mechanism is the aggregate interlock (Vecchio and Collins, 1986; Bentz et al., 2006). The critical shear displacement method (CSDM) (Yang, 2014; Yang et al., 2017) assumes that the delamination crack, which is at the level of flexural reinforcements, is the main trigger for shear failure developing, thus signifying the aggregate interlock effect. A fracture mechanics-based model accounts for residual concrete tensile stress after concrete cracking (Bazant and Kim, 1984; Ghannoum, 1998). The crack sliding shear model (CSSM) is based on a plasticity solution (i.e., upper and lower bound limit analysis theorem) (Fisker and Hagsten, 2016). CSSM thus accounts for the effect of concrete cracking and applies the tensile stress criterion to the flexural cracks' tips, which connect with a shear crack (Tue et al., 2014). Critical shear crack theory (CSCT) includes several shear mechanisms: residual tensile stress in the shear crack, aggregate interlock, and dowel action in one united failure criterion (Muttoni and Fernández Ruiz, 2019). The multi-action model (MAM) is based on several shear mechanisms, including but not limited to the compression chord. Reineck's model includes all shear mechanisms, especially, the compression zone direct shear mechanism in a kinematically consistent manner (Reineck, 1991). This model is based on the equilibrium between both internal and the external stresses due to shear acting upon cracked concrete teeth. The most recent model is shear crack propagation theory (SCPT), which predicts crack propagation and stresses in uncracked concrete, different shear mechanisms, and stresses at the tip of the crack over the loading history (Classen, 2020). However, SCPT is more of a tool for targeting the mechanical bases of one-way shear in steel-RC elements, to be implemented for developing design models.

Previous experimental studies have shown that the shear behavior of concrete elements can be clarified into four categories based on the shear span-to-depth ratio: 1) short elements (i.e., a/d < 1); 2) deep elements (i.e., 1< a/d <2.5); 3) flexure shear dominated elements (i.e., 2.5< a/d <5.0); 4) flexure dominated elements (i.e., 5.0 < a/d). In both short and deep elements, the behavior is dominated by the arch action, while the flexure and shear element is not.

This current study developed a physically based model for FRP-RC slender elements under one-way shear. The work is part of extensive research that aims to investigate the strength of reinforced concrete elements under shear, punching shear, and torsion (Deifalla and Ghobarah, 2010a; Deifalla and Ghobarah, 2010b; Deifalla et al., 2013; Deifalla et al., 2014; Deifalla and Ghobarah, 2014; Deifalla, 2015; Deifalla et al., 2015; Hassan and Deifalla, 2015; Elmeligy et al., 2017; Deifalla, 2020b; Deifalla, 2020c; Deifalla, 2021a; Ali et al., 2021; Deifalla, 2021b; Deifalla, 2021d; Ebid and Deifalla, 2021; Alkhatib and Deifalla, 2022; Deifalla, 2022; Deifalla and Salem, 2022; Salem and Deifalla, 2022). Many of these include the shear strength of FRP-reinforced concrete elements (Ali et al., 2021; Ebid and Deifalla, 2021). Ali et al. (2021) assessed the available design codes and provided a regression model. Ebid and Deifalla (2021) developed a machine learning model. The current study aims to develop a mechanical model based on the concept of plasticity. The CSSM applies to special cases of one-way shear and punching shear and was thus selected for this study. The original CSSM did not address the shear strength of FRP-RC beams and is only applicable to steel-RC beams. Thus, extending it, based on the experimental database, to FRP-RC beams is a significant refinement. A comprehensive literature review for experimental testing of elements under one-way shear was conducted. The CSSM was refined (RCSSM) to model behavior, and a new mechanical model is proposed for FRP-RC slender elements under one-way shear. A few models were selected from the literature to compare to the developed model; however, a comprehensive assessment of existing shear models for FRP-RC slender elements is not within the scope of this study. The RCSSM was used to compute the element's strength and compare it with existing models in the literature. Concluding remarks are outlined and discussed.

2 Experimental database

The present study adopts the most comprehensive database for FRP-RC beams available, consisting of 420 specimens tested in 57 studies (Ali et al., 2021; Ebid and Deifalla, 2021). Further details of the database are available in previous studies (Ali et al., 2021; Ebid and Deifalla, 2021). All these experimental tests utilized FRP as the flexure reinforcement. All elements were four-point static loading, which failed in shear. Shear strengthening and retrofitting using FRP is out of the scope for this study. Table 1 show the frequency distribution of the mechanical and geometrical parameters of the test specimens while the details of all data are available in the supplementary file at the end of the paper. Figure 1 shows the frequency of the values used for the effective depth (d), the compressive strength of concrete (f_c'), the flexural reinforcement ratio (ρ), and FRP's Young's modulus (E). The scope of this study includes slender

TABLE 1 Database of parameters for slender FRP-RC elements under shear.

Source	Range
Database size	420
Studies in the database	57
f_c (MPa)	20–93
b (mm)	89–1830
d (mm)	73–938
a (mm)	299.6–3096
a/d	1.08–16.2
ρ_f (%)	0.09–3.98
E_f (GPa)	29–192

elements which are either flexure shear-dominated or flexure-dominated elements. Thus, the database was filtered to eliminate short and deep elements—defined as those with a shear span-to-depth ratio value of less than 2.5. Hence, a total of 278 specimens were used in this study. The developed models and conclusions in the current study are limited to slender elements and are not necessarily applicable for short and deep elements. Although FRP manufacturing and products have improved significantly over the years, the model depends on FRP's mechanical properties, which are evaluated specifically for the FRP implemented in each research study; thus, the model analysis is not dependent on the quality of the FRP.

3 Assessment of selected models

Several methods have been developed over the last four decades for FRP-RC beams. The well-known design guide for FRP (ACI) (ACI-440.1R-15, 2015) is based on Tureyen and Frosh's model (Tureyen et al., 2006). In addition, a few mechanical models were found in the literature that address the shear of slender FRP-reinforced concrete elements. These are based on the following well-known shear models: 1) the M model (Mari et al., 2014), which is based on the compression chord model; 2) the DN model (Dhahir and Nadir, 2018), which is based on the compression field model; 3) the B model (Baghi et al., 2018), which is based on the modified compression field theory (MCFT) (Bentz et al., 2010). The details of these models are out of the scope of this study, and any further details about the application and derivation of these models can be found in the original manuscript (ACI-440.1R-15, 2015; Tureyen et al., 2006; Mari et al., 2014; Dhahir and Nadir, 2018; Baghi et al., 2018; Bentz et al., 2010). Table 2 shows the five methods selected: ACI, M, DN, and B.

3.1 Overall

Figure 2 shows measurements against calculated strength using the ACI, M, DN, and B methods, and the ideal 45-degree line as well as the best-fit-line and the χ factor, which is calculated as the inverse of the best-fit-line slope. χ is an indication of the over- or underestimation of the used method. Table 3 shows the statistical measures for the SR (i.e., the measured divided by the calculated strength) using different methods as well as the coefficient of

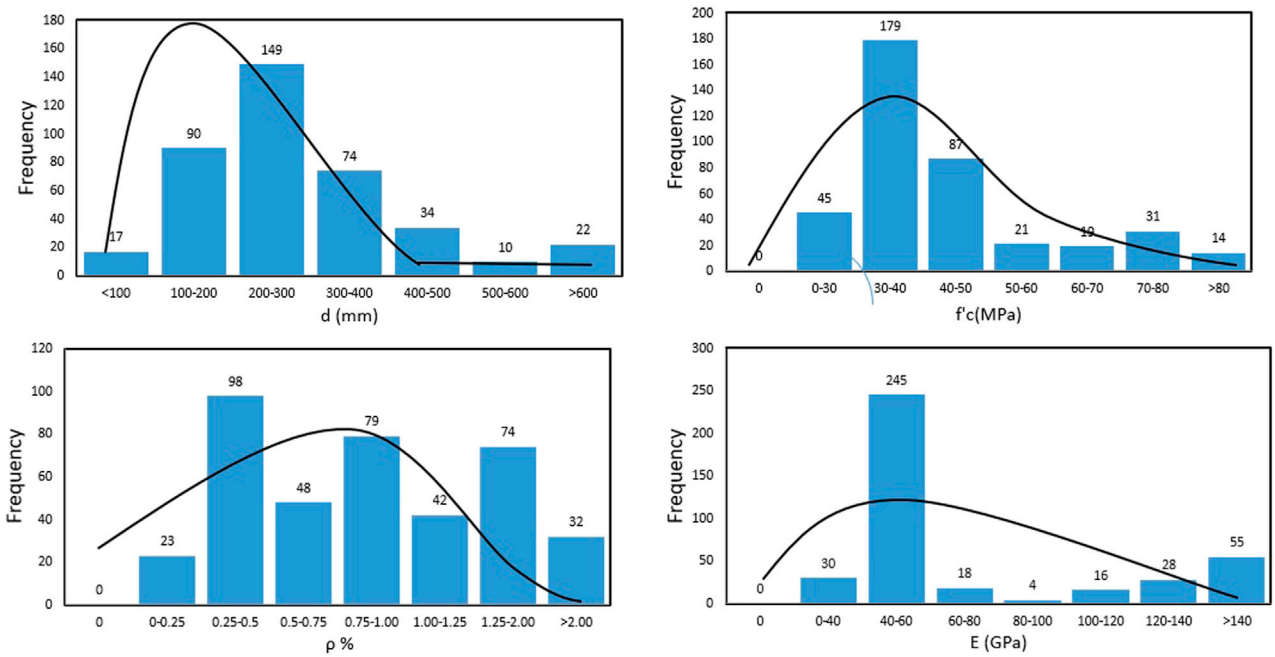

FIGURE 1
Database frequency distribution.

TABLE 2 Summary of selected model and design codes.

Method	Shear resistance, V	Symbols
ACI (ACI-440.1R-15, 2015)	Based on the model by Tureyen and Frosh (Tureyen et al., 2006), the ACI design code for conventional steel RC was modified such that: $0.4\left(\sqrt{2n\rho + (n\rho)^2} - n\rho\right)\sqrt{f_c'}bd$	$n = \frac{E_f}{E_c}$
M model (Mari et al., 2014)	Based on the compression chord model, the model was developed such that: $\xi[(1.072 - 0.01n)\frac{c}{d} + 0.036]f_{ct}bd$	$\xi = 1.2 - 0.2\frac{a}{d}$ $d\ \frac{c}{d} = n\rho\left(-1 + \sqrt{1 + \frac{2}{n\rho}}\right)$
DN model (Dhahir and Nadir, 2018)	Based on the compression field, the model was developed such that: $AE\left(\frac{-2.58 + \sqrt{7.18 + \frac{10506(0.15l_b + 0.72c)bf_c'}{AE}}}{5253}\right)$	$V \geq 0.14(0.15l_b + 0.72c)bf_c'$
B model (Baghi et al., 2018)	Based on the MCFT (Bentz et al., 2010), the model was developed such that: $0.07\left(\frac{E\rho b}{f_c' d}\right)\sqrt{f_c'}\,bd$	$0.05\sqrt{f_c'}\,bd \leq V \leq 0.3\sqrt{f_c'}bd$

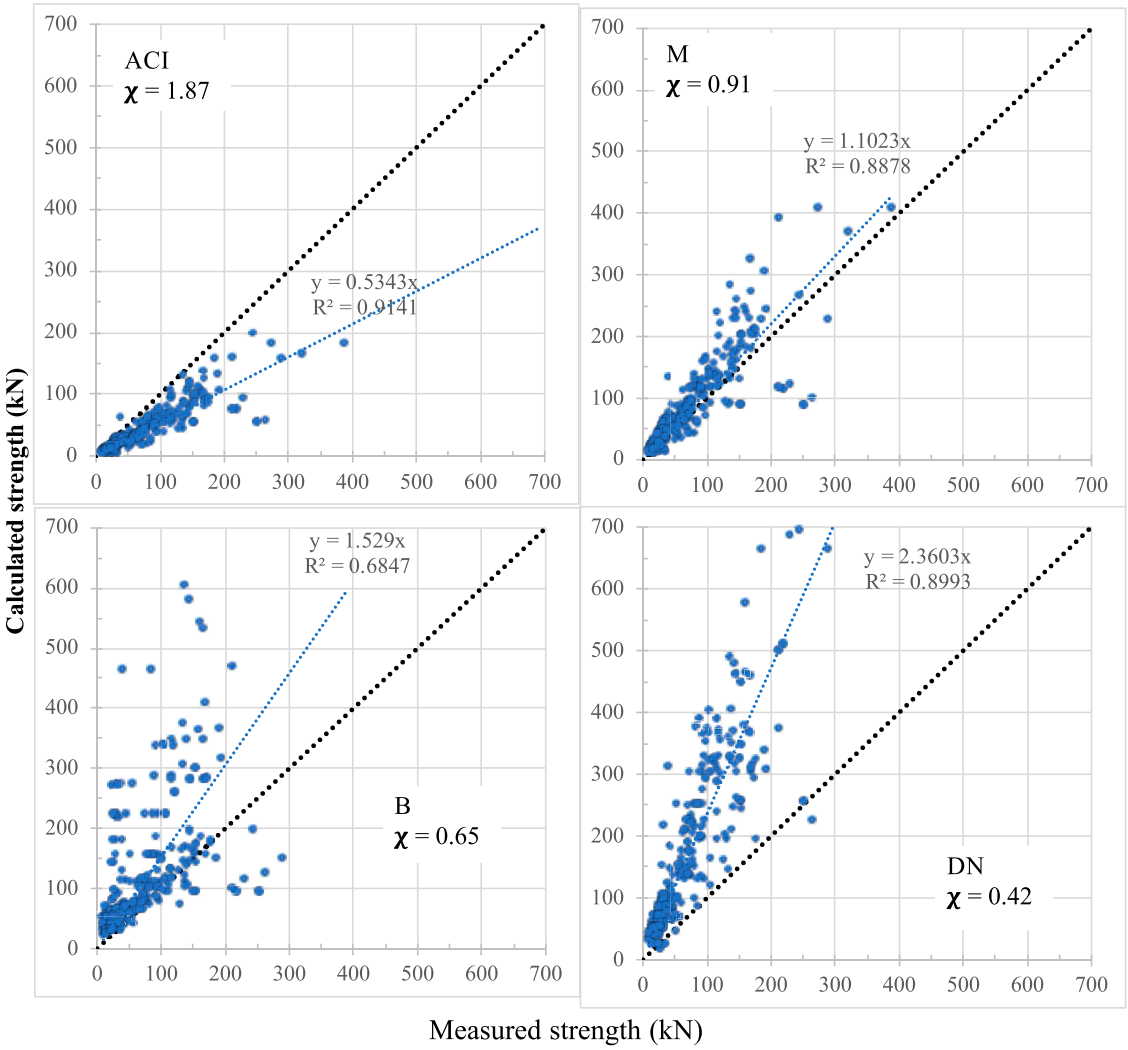

FIGURE 2
Calculated versus measured strength for existing selected models.

correlation between the calculated and measured strengths. The SR statistical measures include the minimum, maximum, average, coefficient of variation, and median. ACI is overly conservative, with a SR average value of 2.02 and a χ factor value of 1.87. The B model is the least conservative, with a SR average value of 0.46 and a χ factor value of 0.43. For the other models, the SR average value ranged 0.61–0.92 and the χ factor ranged 0.50–1.50. For consistency, the coefficient of variation ranged 42%–53%, showing a serious lack

TABLE 3 Statistical measures for SR.

	ACI	M	DN	B
Mean	2.02	0.93	0.72	0.46
C.O.V.	41%	41%	51%	43%
L.L. 99%	1.92	0.88	0.68	0.44
Minimum	0.66	0.31	0.09	0.13
Maximum	7.75	3.04	2.68	1.68
Median	1.82	0.83	0.68	0.41
Correlation coefficient	0.90	0.86	0.66	0.88

TABLE 4 Correlation coefficient between various methods and variables.

	ACI	M	DN	B
Size	0.04	0.28	0.82	0.02
Concrete compressive strength	−0.09	−0.12	−0.35	−0.12
Flexure reinforcement axial rigidity	−0.40	−0.44	−0.01	0.18

of consistency. For safety, the lower 95% is calculated for the ACI; M is above 0.85, which is considered reasonable. However, that calculated for the B and DN models is lower than 0.85, which is needed for the higher safety factor for the purpose of design. The coefficient of correlation between measured strength and that calculated using various methods had values of 0.90, 0.86, 0.66, and 0.88 for the ACI, M, DN, and B methods, respectively, Thus, the strength calculated using various models is highly correlated to experimental measurements; however, the ACI, M, and B models are strongly correlated compared to DN.

3.2 Against size

Table 4 shows the coefficient of correlation between measured and calculated strengths for selected methods against element size. The correlation coefficient between size and calculated SR for ACI, M, DN, and B was 0.04, 0.28, 0.82, and 0.02, respectively. Thus, the calculated SR for all models, excepting DN, is weakly correlated to size compared to the DN model. In addition, Figure 3 shows the calculated SR for the ACI, M, DN, and B models against size and best-fit-line for each model. The best-fit-line slope for the calculated SR for the ACI, M, DN, and B models against size are 2.0E-4, 6.0E-4, 18E-4, and 0.3E-4, respectively. In all models, safety increases with increased concrete compressive strength. DN is less consistent with size than other models and needs further investigation into its size effect.

3.3 Against concrete compressive strength

From Table 4, the correlation coefficient between concrete compressive strength and calculated SR for ACI, M, DN, and B was −0.09, −0.12, −0.35, and −0.12, respectively. Thus, the calculated SR for all models except DN is weakly correlated with concrete compressive strength. In addition, Figure 4 shows the calculated SR for the ACI, M, DN, and B models against concrete compressive strength as well as the best-fit-line for each model. The best-fit-line slope for the calculated SR for the ACI, M, DN, and B models against concrete compressive strength is -47E-4, -28E-4, -81E-4, and -15E-4, respectively. For all models, safety decreases with increased concrete compressive strength. DN is less consistent with concrete compressive strength than other models, and needs further investigation into its concrete compressive strength.

3.4 Against flexure reinforcement axial rigidity

From Table 4, the correlation coefficient between flexure reinforcement axial rigidity and calculated SR for ACI, M, DN, and B was −0.40, −0.44, −0.01, and 0.18, respectively. Thus, the calculated SR for the DN and B methods is weakly correlated compared to the ACI and M models; they thus need further investigation into flexure reinforcement axial rigidity. In addition, Figure 5 shows the calculated SR for the ACI, M, DN, and B models against flexure reinforcement axial rigidity as well as the best-fit-line for each model. The best-fit-line slope for the calculated SR for the ACI, M, DN, and B models against flexure reinforcement axial rigidity is −0.69, −0.35, −0.006, and 0.07, respectively. For all models except B, safety decreases with increased flexure reinforcement axial rigidity. This could be because existing models underestimate the dowel action component of lower values for flexure reinforcement axial rigidity. The ACI is less consistent with flexure reinforcement axial rigidity than other models and needs further investigation into its flexure reinforcement axial rigidity.

4 Refinement of CSSM (RCSSM)

In this study, the CSSM was selected as it is based on plasticity and can be used for both shear and punching shear.

4.1 Background of the crack shear sliding model (CSSM)

This section will briefly outline the original CSSM for one-way shear of concrete elements without stirrups. The CSSM is based on plasticity, where lower and upper boundary solutions for beams under shear are developed. Consider a four-point loading on rectangular beams without stirrups.

4.1.1 Upper bound plasticity solution

An upper bound solution assumes that the beam is divided into two regions with a straight yield-line having an inclination angle β with the beam longitudinal axis, as shown in Figure 6 (Nielsen and Bræstrup, 1975). The middle region (I) is assumed to move vertically using a simple displacement field, while the outer region (II) is assumed to not move. Thus, the work equation is such that:

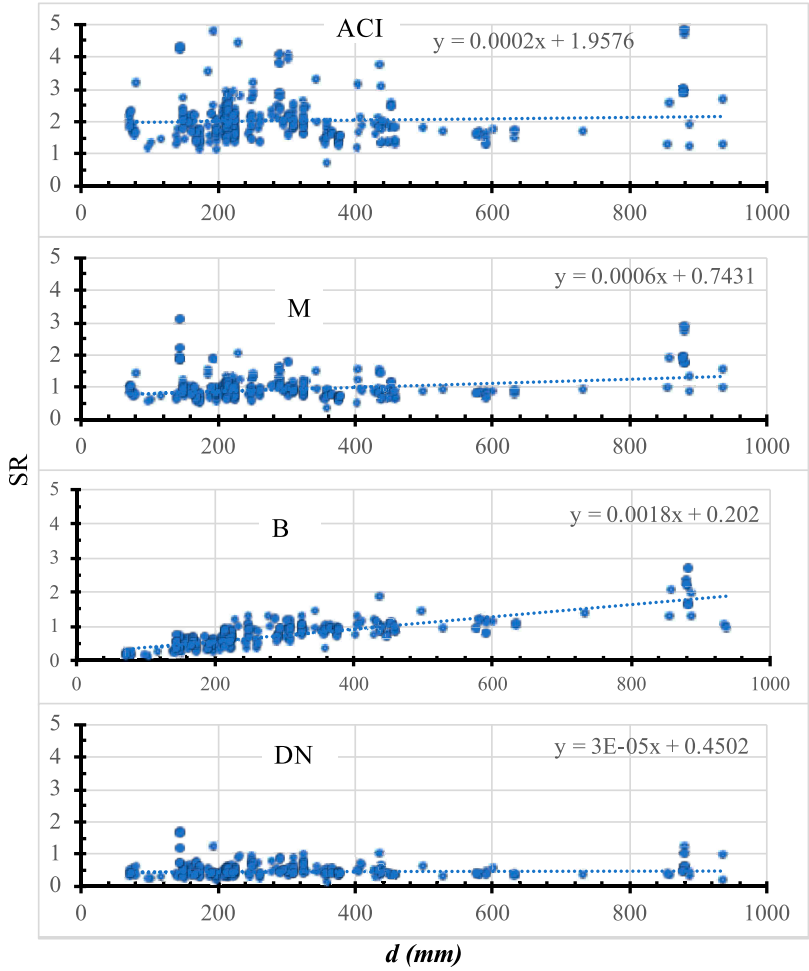

FIGURE 3
SR calculated using selected model versus size.

$$V = \frac{1}{2} f_c b (1 - \cos\beta) \frac{h}{\sin\beta} u \tag{1}$$

which represents the energy dissipation in the concrete, while the longitudinal reinforcements have negligible energy dissipation:

$$\frac{\tau}{f_c} = \frac{V}{bhf_c} = \frac{1}{2}(1 - \cos\beta)\frac{1}{\sin\beta} \tag{2}$$

Finding the minimum V concerning variable β, thus β = 0. However, $\beta \geq \tan^{-1}\frac{h}{a}$; thus the upper bound solution for the shear strength is such that:

$$V = \frac{1}{2} f_c \left[\sqrt{1 + \left(\frac{a}{h}\right)^2} - \frac{a}{h}\right] bh \tag{3}$$

4.1.2 Lower bound plasticity solution

For the case of a four-point bending concrete beam, Figure 7 shows a schematic that can be used to develop a lower bound solution. Shear is transferred *via* a single strut in what is called an "arch mechanism", where axial compression acts on region ABDE. The forces from the reinforcement to the arch are transferred through regions AEF and BCD; consequently, both regions are subjected to biaxial stresses. An anchor plate is used to transfer the anchoring force to the concrete, while the stress is taken as f_c. Thus, the measure of the angle subtended by BDE is π/2, while the maximum shear resistance corresponds to the maximum BC, which is obtained at maximum CD. Since a circle having BE as diameter is the locus of point D, the maximum CD = h/2, where BC is such that:

$$BC = x_o = \frac{1}{2}\left[\sqrt{a^2 + h^2} - a\right] \tag{4}$$

while the maximum shear capacity is such that:

$$V = bx_o f_c \tag{5}$$

which can be written in a form like the upper bound solution such that:

$$V = \frac{1}{2} f_c \left[\sqrt{1 + \left(\frac{a}{h}\right)^2} - \frac{a}{h}\right] bh \tag{6}$$

which is identical to an upper bound solution. This is, therefore, a unique plastic solution for shear resistance.

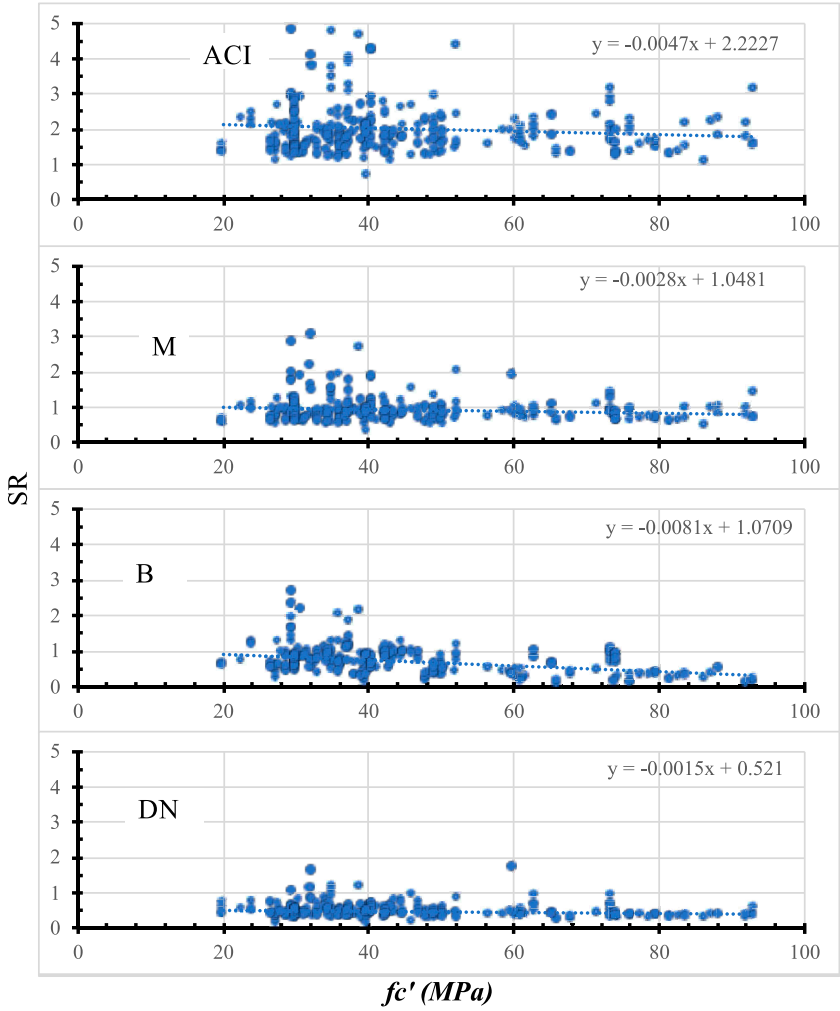

FIGURE 4
SR calculated using selected model versus concrete compressive strength.

4.1.3 Crack sliding model

Figure 8 shows a cracking pattern, starting vertically at the maximum moment cross-section and is then followed by diagonal cracks due to shear. The first crack is usually vertical and close to the point load, starting at the beam bottom soffit; the next one is a diagonal crack directed towards the point load. The load required to initiate diagonal cracks increases with closeness to the support: the cracking load curve. On the other hand, the load resistance for crack sliding decreases with closeness to the support: the shear capacity curve. Therefore, the decrease in the shear span value decreases the angle of inclination of the yield-line and increases the load resistance. The yield-line is defined as the intersection of both the shear capacity and the cracking load. This method predicts much lower shear capacity with respect to the original plastic solution. The yield-line is named the "critical diagonal crack", where the shear capacity is less than the cracking load. The CSCT is based on the observation that yield lines are formed as a transformation from the critical diagonal crack (Muttoni, 1990). This observation was confirmed by measuring the relative displacement along the critical diagonal crack. Initially, the relative displacement along the critical diagonal crack is perpendicular to the crack, while another component of the displacement is formed parallel to the critical diagonal crack. This indicates that the yield line is a transformation of the critical diagonal crack. The cracking moment and the shear capacity of a diagonal crack can be simplified by using an equivalent plastic distribution for the normal stress; the bending moment resistance of concrete element can be calculated as shown in Figure 11. Thus, the cracking moment for concrete is such that:

$$M_{cr} = \frac{1}{2} b h^2 f_{tef} \tag{7}$$

where f_{tef} is the effective tensile strength calculated as $f_{tef} = \nu_t f_t$, where f_t is taken as $0.26 f_c^{2/3}$ and ν_t is taken the constant value of 0.6, and b is the width. In addition, the size effect can be considered using a Weibull factor s(h) on f_{tef}, such that:

$$s(h) = \left(\frac{h}{100}\right)^{-0.3} \tag{8}$$

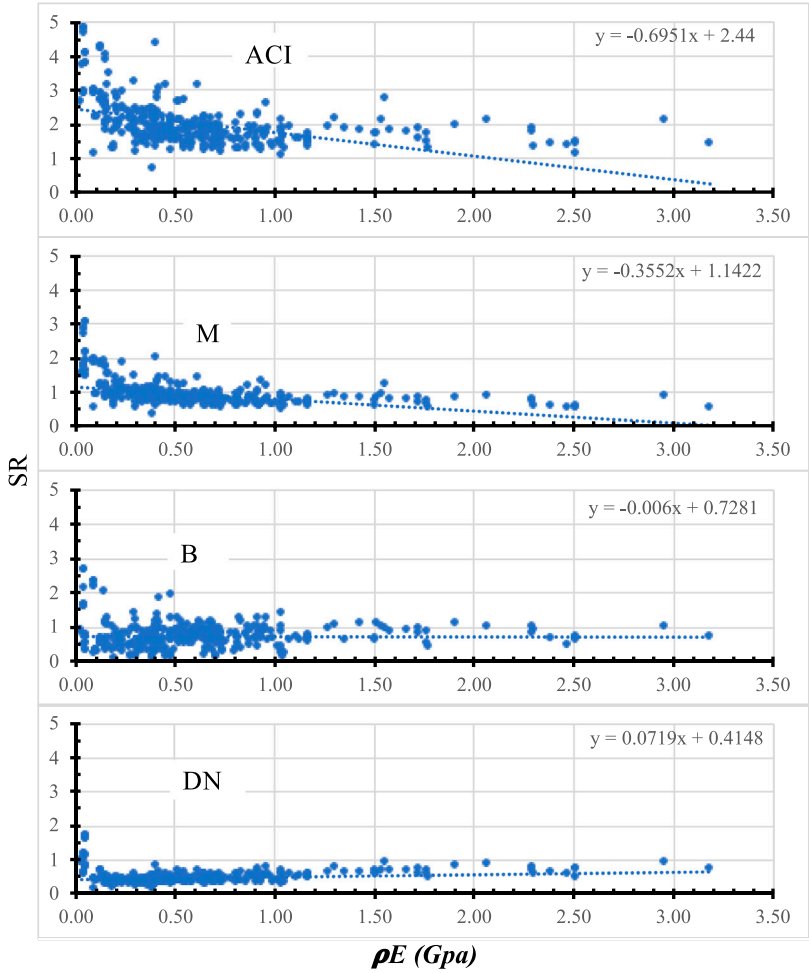

FIGURE 5
SR calculated using selected model versus flexure reinforcement axial rigidity.

where the depth is in mm. Thus, the concrete tensile stress is such that:

$$f_{tef} = 0.6f_t\, s(h) \tag{9}$$

For a concrete element with inclined cracks shown in Figure 9, assuming a straight-line from point A to point B, a statically equivalent uniform tensile stress (f_{tef}) equivalent to the uniform tensile stresses along the curve from point A to point B. Thus, taking the moment equilibrium at point A, the cracking load is calculated such that:

$$M_{cr} = \frac{1}{2}bh^2\left[1 + \left(\frac{x}{h}\right)^2\right]f_{tef} \tag{10}$$

where x is the critical diagonal crack horizontal component.

Shear resistance is reached due to the failure along the two diagonal yield-lines and the upper face of the reinforcements in tension, which can be calculated if the yield-line could be simplified into a straight line, as shown in Figure 10. In addition, an over-RC element can be assumed; thus, the relative horizontal displacement along the yield-lines and the tensile failure at the reinforcement are negligible.

Hence, replacing a with $x = a - x'$ in the upper bound plasticity solution, shear resistance (V) may be calculated such that:

$$V(x) = \frac{1}{2}f_c\left[\sqrt{1 + \left(\frac{x}{h}\right)^2} - \frac{x}{h}\right]bh \tag{11}$$

The cracking load (V_{cr}) is calculated from M_{cr} while neglecting the contribution of the longitudinal flexure reinforcement, such that:

$$V_{cr}(x) = \frac{1}{2}\frac{b[h^2 + x^2]f_{tef}}{(a + L_o/2)} \tag{12}$$

where L_o is the support length. Therefore, the critical shear crack location and the minimum shear strength can be calculated by equating both the V_{cr} and the V. The calculations are numerically long; thus, for the purpose of design, ignoring the support plate width (L_o) [75], the following equation can be used to find the critical crack position, such that:

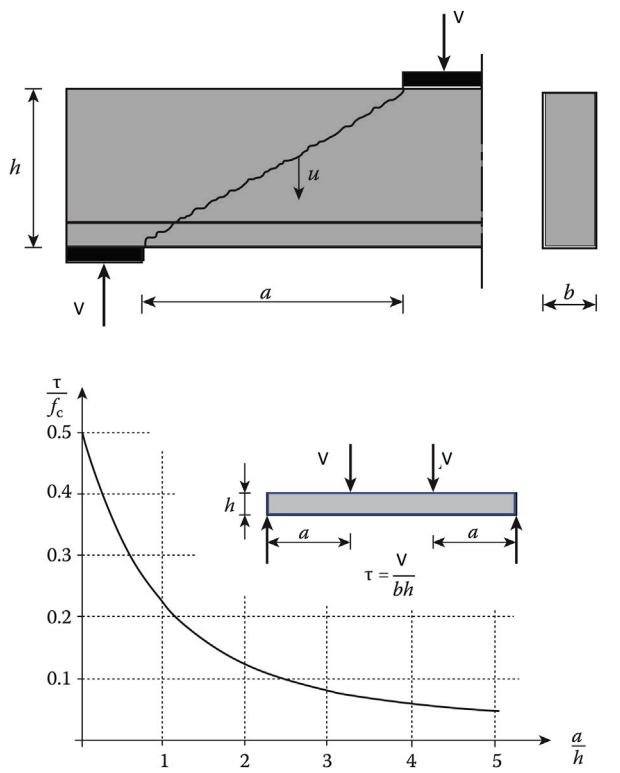

FIGURE 6
Upper bound solution of four-point loading beam.

$$\left(\frac{x}{h}\right)^3 + \frac{x}{h} - 4\frac{\tau_c}{f_{tef}}\frac{a}{h} = 0 \tag{13}$$

In addition, the calculated shear strength is compared with the measured ones; thus, a softening factor v is proposed such that:

$$v = v_s v_o \tag{14}$$

$$v_s = 0.5 \tag{15}$$

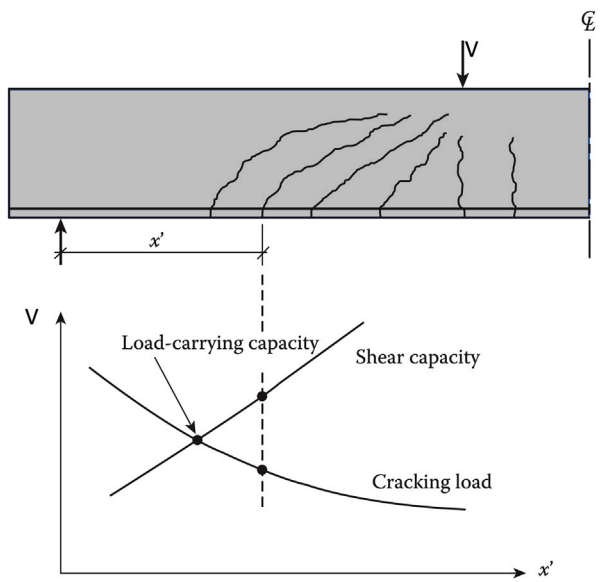

FIGURE 8
Cracking of beams without stirrups.

$$v_o = \frac{0.88}{\sqrt{f_c{}'}}\left(1 + \sqrt{\frac{1000}{h}}\right)(1 + 0.26\rho) \tag{16}$$

where v_s is a reduction factor for the sliding, and $f_c{}'$ is the concrete compressive strength in MPa, h in meters, and ρ is the flexure reinforcement ratio in percentage. The shear resistance can be simplified such that:

$$V(x) = \tau_c \frac{2}{(x/h)} bh \tag{17}$$

where

$$\tau_c = \frac{1}{2}\left[\sqrt{5} - 2\right] v_s v_o f_c \tag{18}$$

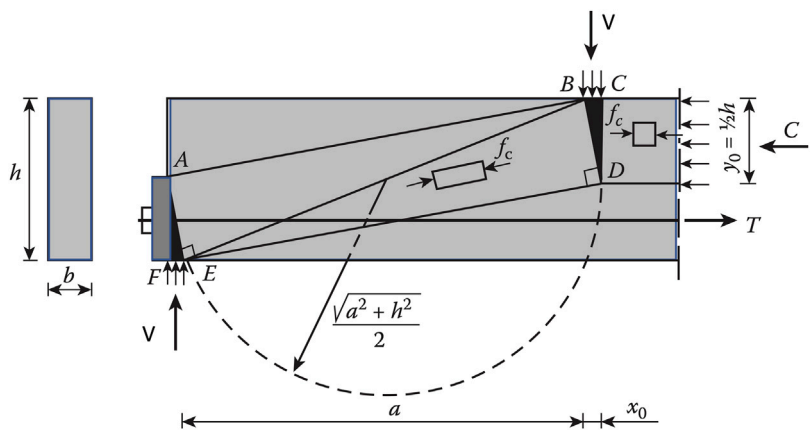

FIGURE 7
Lower bound solution for beam without stirrups.

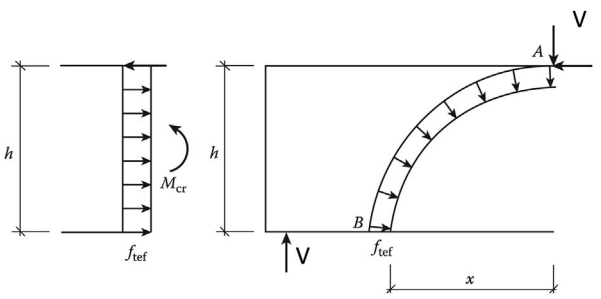

FIGURE 9
Stress distribution across diagonal crack.

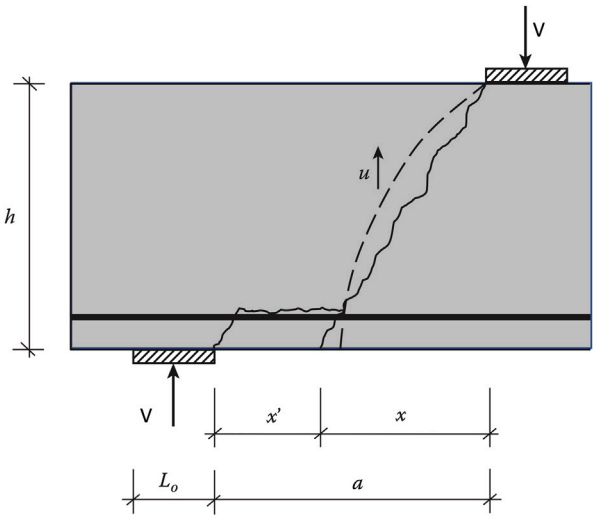

FIGURE 10
Shear failure of a concrete beam with four-point bending loading.

4.2 Model refinement

Based on the observed FRP-RC elements' behavior, the FRP-RC beams' different from the steel RC elements is the variable Young's modulus for FRP, or it is different in the axial rigidity of FRP reinforcements (Hassan and Deifalla, 2015; Ali et al., 2021; Ebid and Deifalla, 2021). Thus, two refined models are proposed—RCSSM-1 and RCSSM-2—where the effect of Young's modulus and FRP axial rigidity, respectively, are included.

4.2.1 First model

In this model, Young's modulus was included in the CSSM using multivariable non-linear regression (RCSSM-1); thus, the shear resistance is such that:

$$V(x) = \tau_c \frac{2}{(x/h)} bh\left(0.87\left(\frac{E_f}{E_s}\right)^{0.2}\right) \tag{19}$$

where E_f is FRP's Young's modulus in GPa, and E_s is steel's Young's modulus in GPa.

4.2.2 Second model

In this model, the flexure re/inforcement axial rigidity was included in the CSSM using multivariable non-linear regression (RCSSM-2); thus, the shear resistance is such that:

$$V(x) = \tau_c \frac{2}{(x/h)} bh\left(0.80\left(\rho\frac{E_f}{E_s}\right)^{0.11}\right) \tag{20}$$

where E_f is FRP's Young's modulus in GPa, and E_s is steel's Young's modulus in GPa.

5 Assessment of the RCSSM

The developed model was assessed by comparing its performance to that of the selected models with respect to the overall performance of the selected parameter.

5.1 Overall

Figure 11 shows the measured strength against the calculated strength using the CSSM, RCSSM-1, and RCSSM-2 methods, respectively, as well as the ideal 45-degree line, and the best-fit-line and the χ factor. Table 5 shows the statistical measures for the calculated SR for different methods. The CSSM model is the least conservative, with an SR average value of 0.71 and a χ factor value of 0.707. For the proposed models, the SR average value is 1.03 and the χ factor value is 1.06. For consistency, the coefficient of variation for all models ranged between 24% and 26%, showing good consistency. For safety, the lower 95% calculated for the RCSSM-1 and RCSSM-2 is above 0.85, which is considered reasonable. However, that calculated for the CSSM is lower than 0.85, which needs a higher safety factor for the purpose of design.

5.2 Against size

Table 6 shows the coefficient of correlation between measured strength and that calculated using various methods against size. The correlation coefficient between size and calculated SR for ACI, M, DN, B, CSSM, RCSSM-1, and RCSSM-2 is 0.04, 0.28, 0.82, 0.02, 0.13, 0.19, and 0.24, respectively. Thus, the calculated SR for the proposed models is weakly correlated to size. In addition, Figure 12 shows the calculated SR for ACI, M, DN, and B models against the size as well as the best-fit-line for each model. The best-fit-line slope for the calculated SR for ACI, M, DN, B, CSSM, RCSSM-1, and RCSSM-2 against size is 2.0E-4, 6.0E-4, 18E-4, 0.3E-4, 1E-4, 2E-4, and 3E-4. For all proposed models, safety increases with increased concrete compressive strength. The proposed models are consistent in size compared to other models.

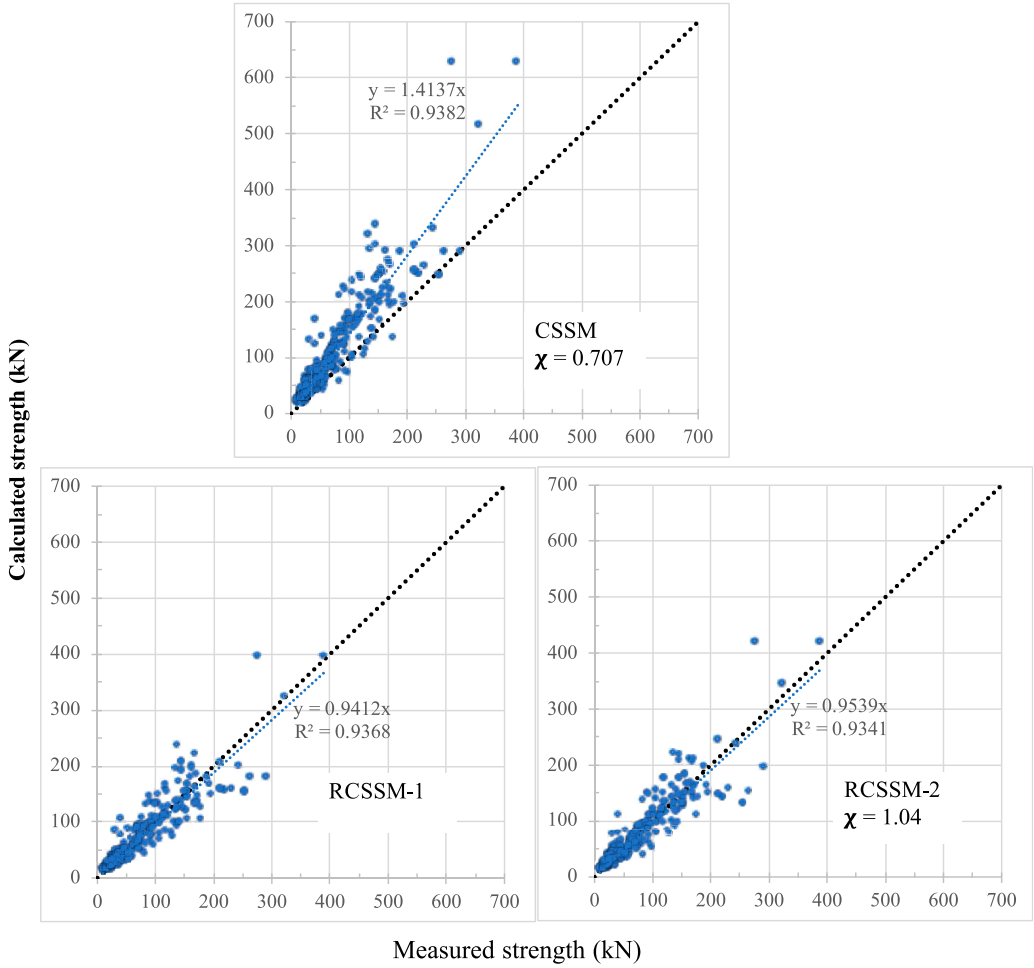

FIGURE 11
Calculated versus measured strength of proposed models.

TABLE 5 Statistical measures for calculated SR for proposed models.

	CSSM	RCSSM-1	RCSSM-2
Mean	0.70	1.03	1.03
C.O.V.	26%	24%	25%
L.L. 99%	0.68	1.01	1.00
Minimum	0.25	0.38	0.37
Maximum	1.46	1.91	2.19
Median	0.66	1.01	0.99
Correlation coefficient	0.92	0.92	0.92

TABLE 6 Correlation coefficient between proposed models and variables.

	CSSM	RCSSM-1	RCSSM-2
Size	0.13	0.19	0.24
Concrete compressive strength	−0.27	−0.29	−0.35
Flexure reinforcement axial rigidity	0.49	0.32	0.16

5.3 Against concrete compressive strength

Table 6 shows the coefficient of correlation between measured and calculated strength for the selected methods against concrete compressive strength. The correlation coefficient between concrete compressive strength and calculated SR for CSSM, RCSSM-1, and RCSSM-2 is −0.27, −0.29, and −0.35, respectively. Thus, the calculated SR for the proposed models is moderately correlated to concrete compressive strength. In addition, Figure 13 shows the calculated SR for CSSM, RCSSM-1, and RCSSM-2 against concrete compressive strength as well as the best-fit-line for each model. The best-fit-line slope for the calculated SR for CSSM, RCSSM-1, and RCSSM-2 against concrete compressive

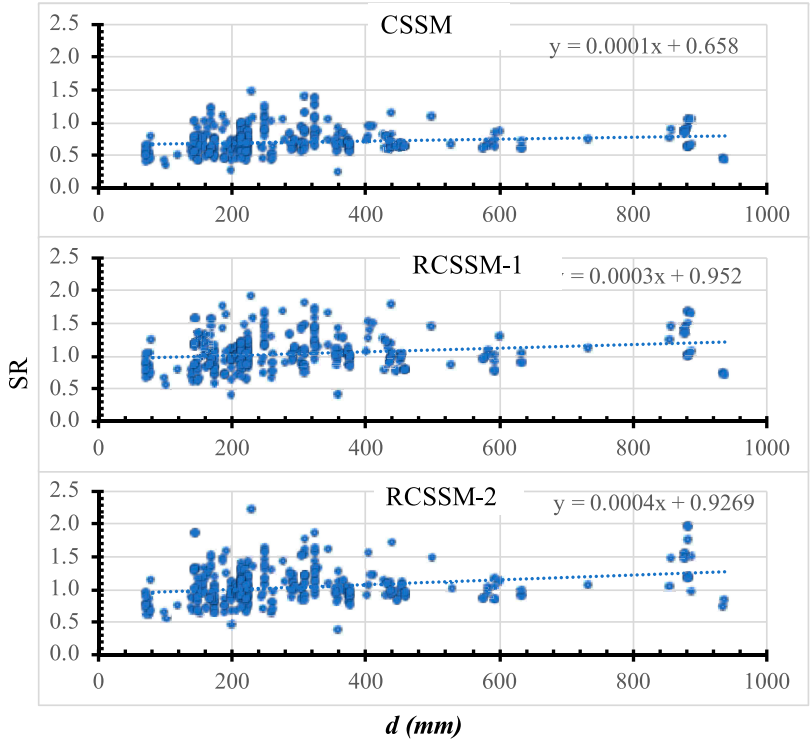

FIGURE 12
SR calculated using proposed models versus size.

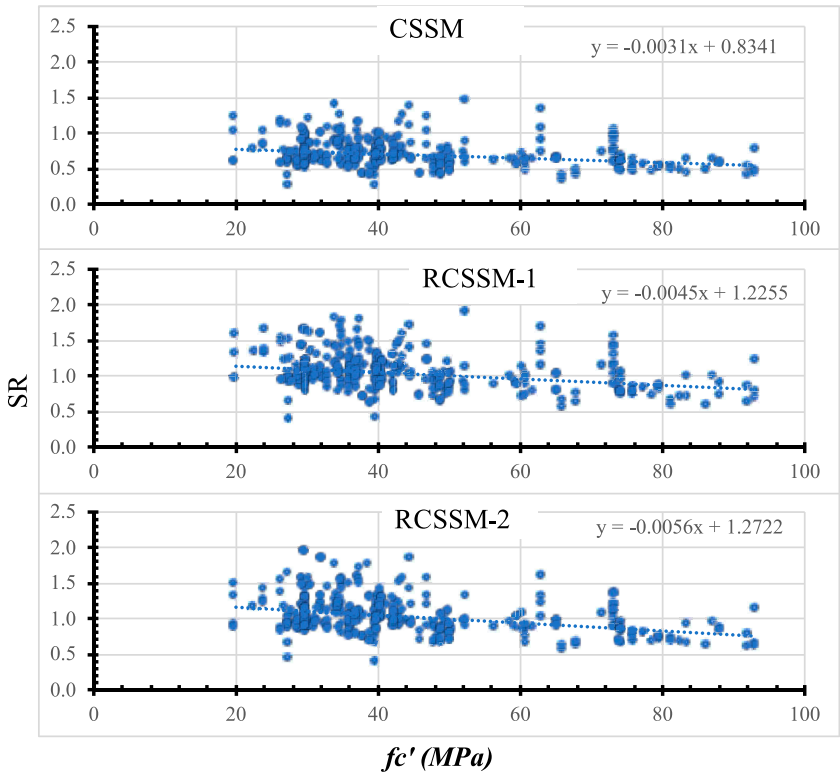

FIGURE 13
SR calculated using proposed models versus concrete compressive strength.

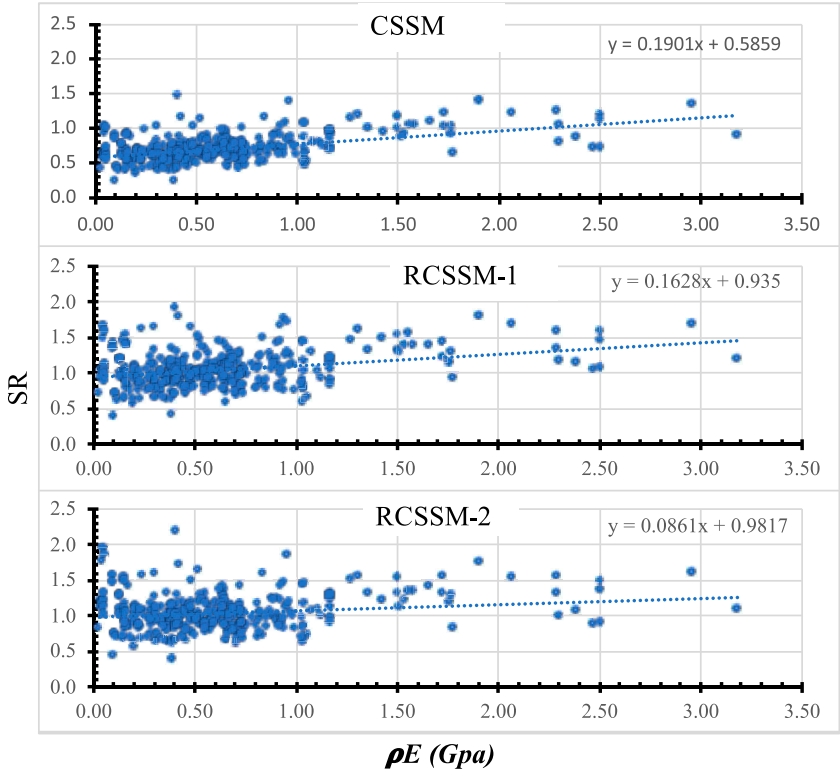

FIGURE 14
SR calculated using proposed models versus flexure reinforcement axial rigidity.

strength is 31E-4, 45E-4, and 56E-4. For proposed models, safety increases with increased concrete compressive strength—consistent with concrete compressive strength compared to other models.

5.4 Against flexure reinforcement axial rigidity

Table 6 shows the coefficient of correlation between measured and calculated strength for the selected methods against flexure reinforcement axial rigidity. The correlation coefficient between flexure reinforcement axial rigidity and calculated SR for ACI, M, DN, B, CSSM, RCSSM-1, and RCSSM-2 is 0.40, 0.40, −0.01, 0.18, 0.49, 0.32, and 0.16, respectively. Thus, the calculated SR for RCSSM-2 is more weakly correlated to the flexure reinforcement axial rigidity than RCSSM-1 and CSSM. In addition, Figure 14 shows the calculated SR for CSSM, RCSSM-1, and RCSSM-2 models the flexure reinforcement axial rigidity as well as the best-fit-line for each model. The best-fit-line slope for the calculated SR for ACI, M, DN, B, CSSM, RCSSM-1, and RCSSM-2 against flexure reinforcement axial rigidity is −0.69, −0.35, −0.006, 0.07, 0.19, 0.16, and 0.08. For all proposed models, safety increases with increased flexure reinforcement axial rigidity. RCSSM-1 is more consistent with flexure reinforcement axial rigidity than RCSSM-1 and CSSM.

6 Conclusion

This study selected five methods and evaluated them with respect to an intensive experimental database; it concluded that:

- ACI is overly conservative, while the B model is the least conservative.
- The DN model is less consistent than other models with respect to the size effect and concrete compressive strength.
- The ACI and M models are less consistent with respect to flexure reinforcement axial rigidity than other models.

In addition, the critical shear sliding model was adapted and further refined to include the effect of Young's modulus to fit the experimentally observed strength. The concluding remarks are:

- Adding the effect of Young's modulus improved the strength predictions with respect to those measured. However, the proposed model was not consistent with flexure reinforcement axial rigidity.

- Adding the effect of flexural reinforcement axial rigidity improved the strength and consistency with respect to flexural reinforcement axial rigidity.

Data availability statement

The original contributions presented in the study are included in the article/Supplementary Material; further inquiries can be directed to the corresponding authors.

Author contributions

Conceptualization, AE-s, TE-S, and AD; methodology, MT, YO, and TE-S; software, MT; validation, AD; formal analysis, AA and YO; investigation, AD and MT; resources, TE-S and AE-s; data curation, AE-s; writing—original draft preparation, AA, TE-S, and AD; writing—review and editing, AE-s, AA, TE-S, YO, AD, and MT; visualization, AD; supervision, AE-s and AD; funding acquisition, AA. All authors have read and agreed to the published version of the manuscript.

Conflict of interest

The authors declare that the research was conducted in the absence of any commercial or financial relationships that could be construed as potential conflicts of interest.

Publisher's note

All claims expressed in this article are solely those of the authors and do not necessarily represent those of their affiliated organizations, or those of the publisher, the editors, and the reviewers. Any product that may be evaluated in this article, or claim that may be made by its manufacturer, is not guaranteed or endorsed by the publisher.

References

ACI-440.1R-15 (2015). *Guide for the design and construction of concrete reinforced with FRP bars, A report by ACI committee 440 Farmington Hills*. American Concrete Institute.

Ali, A., Hamady, M., Chalioris, C. E., and Deifalla, A. (2021). Evaluating the shear design equations of FRP-reinforced concrete beams without shear reinforcement. *Eng. Struct.* 235, 112017. doi:10.1016/j.engstruct.2021.112017

Alkhatib, S., and Deifalla, A. (2022). Punching shear strength of FRP-reinforced concrete slabs without shear reinforcements: A reliability assessment. *Polymers* 14, 1743. doi:10.3390/polym14091743

Baghi, H., Barros, J. A., Kaszubska, M., and Kotynia, R. (2018). Shear behavior of concrete beams reinforced exclusively with longitudinal glass fiber reinforced polymer bars: Analytical model. *Struct. Concr.* 19 (1), 162–173. doi:10.1002/suco.201700175

Bazant, Z. P., and Kim, J.-K. (1984). Size effect in shear failure of longitudinally reinforced beams. *ACI J.* 81, 456–468.

Bazant, Z. P., and Planas, J. (1998). *Fracture and size effect in concrete and other quasibrittle materials*. Boca Raton, FL, USA: CRC Press. ISBN 0-849-8284-X.

Bentz, E. C., Massam, L., and Collins, M. P. (2010). Shear strength of large concrete members with FRP reinforcement. *J. Compos. Constr.* 14, 637–646. doi:10.1061/(asce)cc.1943-5614.0000108

Bentz, E. C. (2005). Empirical modeling of reinforced concrete shear strength size effect for members without. *Stirrups. ACI Struct. J.* 102, 232–241.

Bentz, E. C., Vecchio, F. J., and Collins, M. P. (2006). Simplified Modified Compression Field Theory for calculating shear strength of reinforced concrete members. *ACI Struct. J.* 103, 614–624. doi:10.14359/16438

Cavagnis, F. (2017). *Shear in reinforced concrete without transverse reinforcement: From refined experimental measurements to mechanical models*. Ph.D. Thesis. Lausanne, Switzerland: Ecole Polytechnique Fédérale de Lausanne.

Cladera, A., Marí, A., Bairán, J.-M., Oller, E., and Ribas, C. (2017). One-way shear design method based on a multi-action model: A compromise between simplicity and accuracy. *Concr. Int.* 40, 46.

Classen, M. (2020). Shear Crack Propagation Theory (SCPT)–The mechanical solution to the riddle of shear in RC members without shear reinforcement. *Eng. Struct.* 210, 110207. doi:10.1016/j.engstruct.2020.110207

Deifalla, A. (2021b). A mechanical model for concrete slabs subjected to combined punching shear and in-plane tensile forces. *Eng. Struct.* 231 (231), 111787. doi:10.1016/j.engstruct.2020.111787

Deifalla, A. (2021d). A strength and deformation model for prestressed lightweight concrete slabs under two-way shear. *Adv. Struct. Eng.* 24, 3144–3155. doi:10.1177/13694332211020408

Deifalla, A. (2021a). Refining the torsion design of fibered concrete beams reinforced with FRP using multi-variable non-linear regression analysis for experimental results. *Eng. Struct.* 224, 111394. doi:10.1016/j.engstruct.2020.111394

Deifalla, A. (2020b). Strength and ductility of lightweight reinforced concrete slabs under punching shear. *Structures* 27 (2020), 2329–2345. doi:10.1016/j.istruc.2020.08.002

Deifalla, A. (2020c). Torsion design of lightweight concrete beams without or with fibers: A comparative study and a refined cracking torque formula. *Structures* 28, 786–802. doi:10.1016/j.istruc.2020.09.004

Deifalla, A., Awad, A., and El-Garhy, M. (2013). Effectiveness of externally bonded CFRP strips for strengthening flanged beams under torsion: An experimental study. *Eng. Struct.* 56, 2065–2075. doi:10.1016/j.engstruct.2013.08.027

Deifalla, A., and Ghobarah, A. (2014). Behavior and analysis of inverted T-shaped RC beams under shear and torsion. *Eng. Struct.* 62, 57–70. doi:10.1016/j.engstruct.2014.02.011

Deifalla, A., and Ghobarah, A. (2010). Full torsional behavior of RC beams wrapped with FRP: Analytical model. *Compos. Constr.* 14 (3), 289–300. ASCE, May/June 2010. doi:10.1061/(asce)cc.1943-5614.0000085

Deifalla, A., and Ghobarah, A. (2010). Strengthening RC T-beams subjected to combined torsion and shear using FRP fabrics – experimental study. *Compos. Constr.* 14 (3), 301–311. ASCE, May/June 2010. doi:10.1061/(asce)cc.1943-5614.0000091

Deifalla, A., Hamed, M., Saleh, A., and Ali, T. (2014). Exploring GFRP bars as reinforcement for rectangular and L-shaped beams subjected to significant torsion: An experimental study. *Eng. Struct.* 59, 776–786. doi:10.1016/j.engstruct.2013.11.027

Deifalla, A., Khali, M. S., and Abdelrahman, A. (2015). Simplified model for the torsional strength of concrete beams with GFRP stirrups. *Compos. Constr. ASCE* 19 (1), 04014032. doi:10.1061/(ASCE)CC.19435614.0000498

Deifalla, A. (2022). Punching shear strength and deformation for FRP-reinforced concrete slabs without shear reinforcements. *Case Stud. Constr. Mater.* 16, e00925. doi:10.1016/j.cscm.2022.e00925

Deifalla, A., and Salem, N. M. (2022). A machine learning model for torsion strength of externally bonded FRP-reinforced concrete beams. *Polymers* 14, 1824. doi:10.3390/polym14091824

Deifalla, A. (2015). Torsional behavior of rectangular and flanged concrete beams with FRP reinforcements. *J. Struct. Eng.* 141, 04015068. ASCE. doi:10.1061/(ASCE)ST.1943-541X.0001322

Dhahir, M. K., and Nadir, W. (2018). A compression field-based model to assess the shear strength of concrete beams reinforced with longitudinal FRP bars. *Constr. Build. Mater.* 191, 736–751. doi:10.1016/j.conbuildmat.2018.10.036

Ebid, A., and Deifalla, A. (2021). Prediction of shear strength of FRP reinforced beams with and without stirrups using (GP) technique. *Ain Shams Eng. J.* 12 (3), 2493–2510. doi:10.1016/j.asej.2021.02.006

Elmeligy, O., El-Nemr, A. M., and Deifalla, A. (2017). "Reevaluating the modified shear provision of CAN/CSA S806-12 for concrete beams reinforced with FRP stirrups," in *AEI conference 2017* (OKLAHOMA CITY). ASCE. doi:10.1061/9780784480502.027

Fisker, J., and Hagsten, L. G. (2016). Mechanical model for the shear capacity of R/C beams without stirrups: A proposal based on limit analysis. *Eng. Struct.* 115, 220–231. doi:10.1016/j.engstruct.2016.02.035

Ghannoum, W. M. (1998). *Size effect on shear strength of reinforced concrete beams*. Master's Thesis. Montréal, QC Canada: Mc Gill University.

Hassan, M. M., and Deifalla, A. (2015). Evaluating the new CAN/CSA-S806-12 torsion provisions for concrete beams with FRP reinforcements. *Mater. Struct.* 49, 2715–2729. doi:10.1617/s11527-015-0680-9

Hedman, O., and Losberg, A. (1978). "Design of concrete structures with regard to shear forces," in *Shear and torsion: Explanatory and viewpoint papers on model code chapters 11 and 12 prepared by members of CEB commission V*. Editors P. E. Regan and H. P. J. Taylor (Lausanne, Switzerland: International Federation for Structural Concrete), 184–209.

Huber, P., Huber, T., and Kollegger, J. (2016). Investigation of the shear behavior of RC beams on the basis of measured crack kinematics. *Eng. Struct.* 113, 41–58. doi:10.1016/j.engstruct.2016.01.025

Leonhardt, F., Walther, R., and Dilger, W. (1964). *Schubversuche an Durchlauftragern (Zweifeldrige Stahlbetonbalken mit und ohne Schubbewehrung): DAfStb-Heft 163*. Berlin, Germany: Ernst and Sohn.

Mari, A., Cladera, A., Oller, E., and Bairan, J. (2014). Shear design of FRP reinforced concrete beams without transverse reinforcement. *Compos. Part B Eng.* 57, 228–241. doi:10.1016/j.compositesb.2013.10.005

Muttoni, A. (1990). *Die Anwendbarkeit der Plasticitatstheorie in der Bemessung von Stahlbeton, ETH Zurich, Institut Fur Baustatik und Konstruktion*, 176. Bericht Nr.

Muttoni, A., and Fernández Ruiz, M. (2019). From experimental evidence to mechanical modeling and design expressions: The Critical Shear Crack Theory for shear design. *Struct. Concr.* 111, 1464–1480. doi:10.1002/suco.201900193

Muttoni, A., and Fernández Ruiz, M. (2008). Shear strength of members without transverse reinforcement as function of critical shear crack width. *ACI Struct. J.* 105, 163–172.

Nielsen, M. P., and Bræstrup, M. W. (1975). Plastic shear strength of reinforced concrete beams. *Bygningsstat. Medd.* 46 (3), 61–99.

Reineck, K.-H. (1991). Ultimate sheer force of structural concrete members without transverse reinforcement derived from a mechanical model. *ACI Struct. J.* 88, 592–602.

Salem, N. M., and Deifalla, A. (2022). Evaluation of the strength of slab-column connections with FRPs using machine learning algorithms. *Polymers* 14, 1517. doi:10.3390/polym14081517

Tue, N. V., Theiler, W., and Tung, N. D. (2014). Schubverhalten von Biegebauteilen ohne Querkraftbewehrung. *Bet. Stahlbetonbau* 109, 666–677. doi:10.1002/best.201400058

Tung, N. D., and Tue, N. V. (2016). A new approach to shear design of slender reinforced concrete members without transverse reinforcement. *Eng. Struct.* 107, 180–194. doi:10.1016/j.engstruct.2015.04.015

Tureyen, A. K., Wolf, T. S., and Frosch, R. J. (2006). Shear strength of reinforced concrete T-beams without transverse reinforcement. *ACI Struct. J.* 103, 656–663. doi:10.14359/16917

Vecchio, F. J., and Collins, M. P. (1986). The modified compression-field theory for reinforced concrete elements subjected to shear. *ACI Struct. J.* 83, 219–231. doi:10.14359/10416

Yang, Y. (2014). *Shear behaviour of reinforced concrete members without shear reinforcement: A new look at an old problem*. Ph.D. Thesis. Delft, Netherlands: Delft University of Technology.

Yang, Y., Walraven, J., and Uijl, J. d. (2017). Shear behavior of reinforced concrete beams without transverse reinforcement based on critical shear displacement. *J. Struct. Eng.* 143, 1–13. doi:10.1061/(ASCE)ST.1943-541X.0001608

Zararis, P. D., and Papadakis, G. C. (2001). Diagonal shear failure and size effect in RC beams without web reinforcement. *J. Struct. Eng.* 127, 733–742. doi:10.1061/(asce)0733-9445(2001)127:7(733)

Zink, M. (1999). *Zum Biegeschubversagen Schlanker Bauteile aus Hochleistungsbeton Mit und Ohne Vorspannung*. Ph.D. Thesis. Leipzig, Germany: Universitat Leipzig.

Zsutty, T. C. (1968). Beam shear strength prediction by analysis of existing data. *ACI J.* 65, 943–951.